Plasmonic Nanohybrid with Ultrasmall Ag Nanoparticles and Fluorescent Dyes

Gabriele Rainò,[†,*] Thilo Stöferle,[†] Chanhee Park,[‡] Ho-Cheol Kim,[‡,*] Teya Topuria,[‡] Philip M. Rice,[‡] In-Joo Chin,[§] Robert D. Miller,[‡] and Rainer F. Mahrt[†,*]

[†]IBM Research—Zurich, Säumerstrasse 4, 8803 Rüschlikon, Switzerland, [‡]IBM Research—Almaden, 650 Harry Road, San Jose, California 95120-6099, United States, and [§]Polymer Science and Engineering Department, Inha University, 253 Yonghyun-dong, Incheon 402-751, Korea

ABSTRACT We investigate a hybrid nanocomposite combining fluorescent dyes and ultrasmall (<3 nm) silver nanocrystals in a block copolymer micelle. Although the metal nanoparticles are significantly smaller than the electromagnetic skin depth, we observe a modification of the exciton lifetime and the nonradiative energy transfer among the dyes. This behavior is absent in a control experiment with dyes whose energetic levels are far from the plasmonic resonance, establishing the plasmonic nature of the interaction.

KEYWORDS: surface plasmon resonance · block copolymers · fluorescent probes · micelles · fluorescent spectroscopy

Harnessing surface plasmons is a promising route to reduce the dimensions of optical probes and devices deep into the subwavelength domain.[1] Beyond this paramount scaling advantage, engineering plasmon–exciton interaction opens up attractive ways to tailor the electro-optical properties of nanocomposites containing organic and/or inorganic emitters and metal nanocrystals. Previous studies mostly investigated hybrids with nanoparticle sizes (in diameter) between 10 and 100 nm[2−11] owing to the large magnitude of the plasmonic effect and small affinity to aggregation. Only few efforts cover ultrasmall nanocrystals,[12−16] although these are better suited for many applications, for example, in biology, where a minimal invasive integration is required,[12−16] as well as in catalysis,[17,18] nanoimaging,[19,20] sensing,[21,22] and lithographic tools.[23,24]

We focus on the plasmon–exciton interaction occurring among ultrasmall (2–3 nm) silver nanocrystals and fluorescent dyes embedded in micelle structures. Thereby we are able to access the intriguing regime in which the dimensions of the nanoparticles and the characteristic energy transfer distance between the dyes are comparable.

Metal nanoparticles (MNPs) which support a plasmonic resonance in the visible wavelength range are able to alter the absorption and emission properties of an emitter (fluorescent dye) in close proximity to them.[2−11,13,15,25] The metal–emitter interaction can manifest itself by an enhancement or a quenching of the photoluminescence depending on the relative distance between the dye molecule and the metal. It was theoretically predicted[26,27] and later experimentally demonstrated[28,29] that the presence of metal nanoparticles can alter the Förster resonance energy transfer (FRET) mediated by the resonant dipole–dipole interaction between two molecules in close proximity. Important factors affecting the strength of the interaction are the size and shape of the metal nanoparticles, the relative orientation of the dipole moments, and the overlap of the absorption and emission bands of the dye with the plasmon band of the metal.

Although considerable progress has been made in recent years, the plasmon–exciton interaction with ultrasmall metal nanoparticles is largely unexplored owing to the difficulty of synthesizing small and stable metal nanocrystals. In fact, as the diameter decreases, the surface energy increases, thus enhancing the aggregation probability. Recently, Brege *et al.* reported on a new synthesis route based on the micelles of sodium dodecylbenzenesulfonate surfactant and allowing the growth of stable and crystalline copper nanoparticles with an average diameter of about 2 nm.[16] However, no evidence of a plasmonic resonance was observed, which was attributed to the small particle size and/or the presence of a thin copper oxide layer around the particles. Moreover, a critical size of 2.2 nm was found for gold nanocrystals, with an abrupt transition from metallic behavior to a molecular-like regime.[30]

Here, we use a synthesis route that enables the controlled growth of small (2–3 nm) silver particles inside a diblock copolymer micelle together with different dye molecules

* Address correspondence to gra@zurich.ibm.com, hckim@us.ibm.com, rfm@zurich.ibm.com.

Received for review October 11, 2010 and accepted April 25, 2011.

Published online May 02, 2011
10.1021/nn102717z

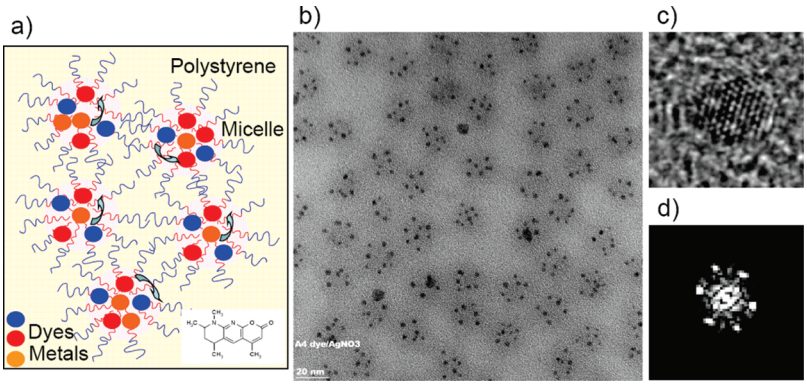

Figure 1. (a) Illustration of the sample used in this work. (b) TEM image of Ag nanoparticles encapsulated in a block copolymer micelle structure. The fluorescent dyes are not visible in this picture. (c) High-resolution TEM image and (d) FFT revealing the crystalline structure of the metal nanoparticles.

(Coumarin and Rhodamine) in close proximity to the metal nanoparticles. Our work demonstrates the occurrence of a plasmon–exciton interaction affecting the exciton lifetime and the nonradiative energy transfer of the dye (Coumarin) in resonance with the plasmon band of ultrasmall Ag nanocrystals, while leaving the emission of a nonresonant dye (Rhodamine) unchanged.

RESULTS AND DISCUSSION

Figure 1a shows a sketch of the micelle structures synthesized in this work. The emitter (organic dye) and metal nanocrystal are confined within nanoscopic space (approximately 20 nm in diameter) using micelles of a block copolymer. A diblock copolymer of polystyrene (PS) and poly(4-vinyl pyridine) (P4VP), PS-*b*-P4VP, was dissolved in toluene. As toluene is a selective solvent for PS, the PS-*b*-P4VP forms micelles with a P4VP core and PS corona in the solution.[31] After stirring, organic dyes were added to the solution. Subsequently, silver nanocrystals are incorporated into the core by micellization and reduction of silver nitrate ($AgNO_3$).[32]

The structure and the chemical composition of the silver nanoparticles were characterized by transmission electron microscopy (TEM) and X-ray photoelectron spectroscopy, respectively. A dilute micelle solution (0.05 wt %) was dropped on a carbon-coated TEM grid (Cu). TEM analysis shows a uniform distribution of distinct and nonaggregated ultrasmall Ag nanoparticles within the micelles, as reported in Figure 1b. High-resolution TEM imaging (Figure 1c) together with fast Fourier transform (FFT) of Ag nanoparticles (Figure 1d) revealed their crystalline nature.

In order to analyze the hybrid system and acquire information also on the organic counterpart, an advanced TEM technique referred to as high angle annular dark-field scanning transmission electron microscopy (HAADF-STEM) has been used.[33,34] The images generated by this technique are essentially incoherent, do not exhibit contrast reversals over a wide range of thicknesses, and are very sensitive to the average atomic number Z of the atomic species in the specimen. Figure 2a shows typical HAADF-STEM images obtained on the samples studied in this work. A much better contrast (compared to bright-field TEM) is obtained, allowing the resolution of the micelle structure and the metal nanoparticles simultaneously. On the basis of these measurements, we estimated that, on average, 7 ± 2 Ag particles are accommodated in each micelle. More interesting, the diameter of the silver particles has been estimated to be around 3 nm, as inferred from Figure 2b. The histogram was obtained measuring diameters for 125 Ag particles from 90 micelles arbitrarily selected.

Moreover, electron energy loss spectra (EELS) can be obtained from the transmitted beam that is not blocked by the HAADF detector. These measurements, reported in Figure 2c, indicate that the micelles contain nitrogen (N) which originates from either the poly (4-vinyl pyridine) or the emitter dye. Comparison of the nitrogen K-edge signal inside the micelle with the lack of nitrogen signal in the regions without micelles leads to the conclusion that both the dyes and the metal particles were efficiently loaded within the micelle structure.

The micelles containing the emitter dye and the Ag nanocrystal were dispersed in PS homopolymer matrix by mixing with PS in toluene solution followed by spin coating onto quartz wafers. The amount of dye was controlled by the mixing composition of PS homopolymer and the dye (and/or nanocrystal) containing micelles.

The metal–emitter interaction was investigated by studying the optical properties of fluorescent dyes in close proximity of the metal nanoparticles. We have chosen the Coumarin dye because of its good spectral overlap with the silver nanocrystals plasmon band (Figure 3a).[3,4,8,9,25]

Figure 3a shows the room-temperature photoluminescence (PL) and PL excitation (PLE) spectra of the Coumarin encapsulated in the micelle structures and of the hybrid composite system including the Coumarin

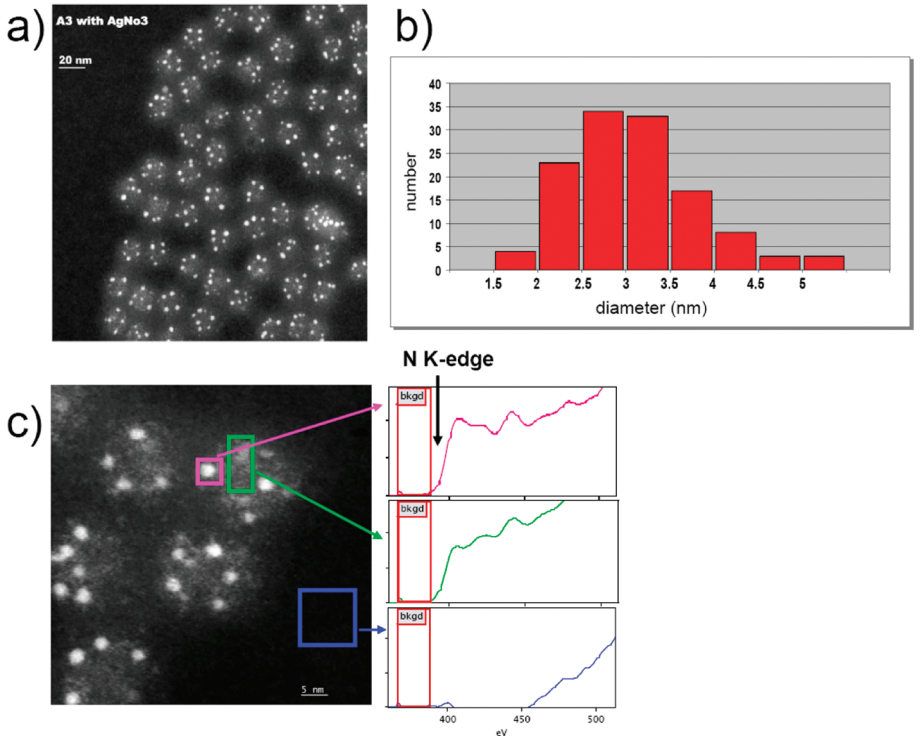

Figure 2. (a) *Z*-contrasted HRTEM images of micelle structures. (b) Size distribution of the Ag nanocrystals. (c) EELS data show that the micelles contain N, which is coming from both poly(4-vinyl pyridine) and the emitter dye.

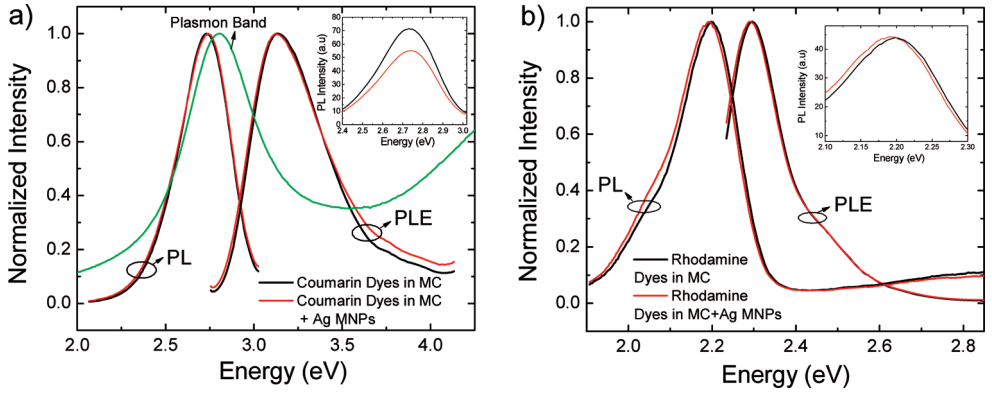

Figure 3. (a) Normalized room-temperature PL and PLE spectra for a sample having only the Coumarin dyes in the micelles (black line) and for a sample combining the same dyes with the metal nanoparticles (red line). The absorption spectrum of a sample containing only Ag nanoparticles is also reported (green line). A clear plasmon resonance peaked at 2.8 eV has been observed. The inset shows the absolute emission intensity of both samples. (b) Control experiments: normalized PL and PLE spectra for Rhodamine dyes dispersed in the micelle structures (black line) and for a dye–MNP composite (red line). The inset shows the absolute PL intensity for both samples.

and the metal nanocrystals. Moreover, the absorption spectrum of Ag particles is reported. The PL spectra of the two systems are virtually identical in terms of energy peak position and relative full width at half-maximum (fwhm). In contrast, the PLE spectra differ slightly at energies higher than 3.5 eV, where a higher relative absorption for the dye–MNP nanohybrid is observed. This effect could be related to the relatively higher contribution of the Ag particles in this spectral range. The inset of Figure 3a shows the absolute PL intensity for both samples. The hybrid system exhibits a lower quantum yield, probably as a result of the interaction with metal nanoparticles. In fact, a very good overlap between the Coumarin PL band and the plasmon band (peaked at 2.8 eV) is clearly observed in Figure 3a. To validate this hypothesis, we performed control experiments by replacing the Coumarin encapsulated in the micelle structures with Rhodamine. We selected Rhodamine because both absorption and emission exhibit no spectral overlap with the silver plasmon band. Again two micelle samples were fabricated in analogy to the Coumarin case. The PL and PLE

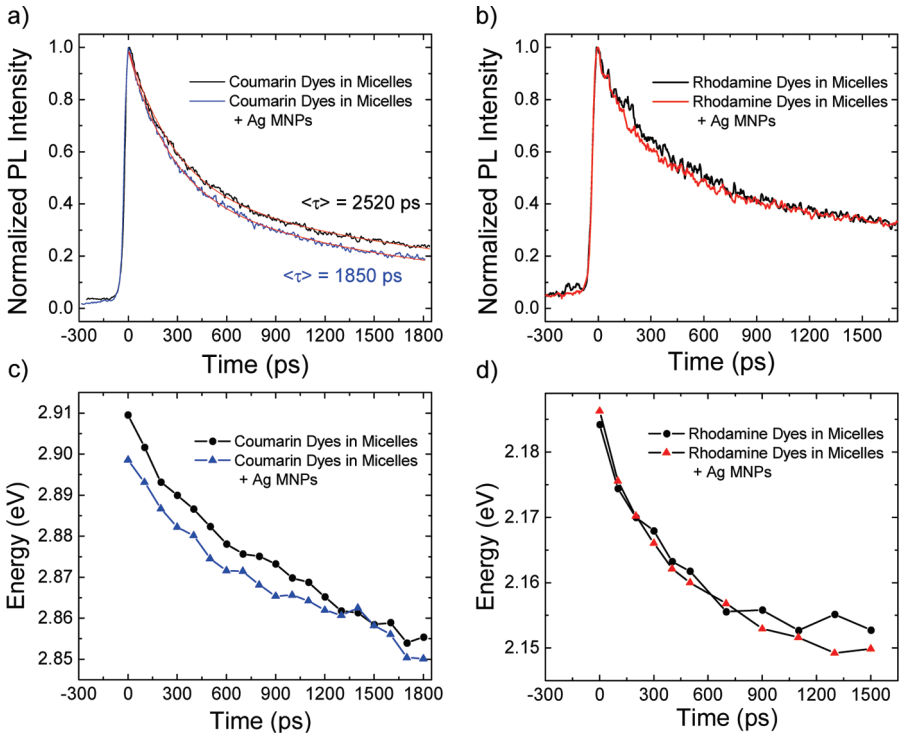

Figure 4. (a) Influence of the plasmon−exciton interaction on the exciton lifetime. Normalized spectrally integrated time-resolved traces for Coumarin (black line) and Coumarin dyes linked to metal nanoparticles (blue line) obtained at a temperature of 6 K. The red lines are the best fit obtained using a biexponential decay function. (b) Control experiments: normalized spectrally integrated time-resolved traces for Rhodamine (black line) and Rhodamine dyes linked to metal nanoparticles (red line) obtained at 6 K. (c) Influence of the plasmon−exciton interaction on the nonradiative energy transfer between an ensemble of dyes within a micelle. Energy peak position *vs* time for Coumarin dyes (black dotted lines) and dyes linked to metal nanoparticles (blue dotted lines) obtained by fitting the spectra to a single Gaussian function. (d) Control experiments: energy peak position *vs* time for Rhodamine dyes (black dotted lines) and dyes linked to metal nanoparticles (red dotted lines).

spectra of these composites are displayed in Figure 3b. Here, both the emission intensity (inset Figure 3b) and the absorption are virtually identical, suggesting the lack of any plasmonic interaction.

To further confirm these results and to establish that such ultrasmall MNPs can indeed alter the emission properties of an emitter, we performed time-resolved experiments. These measurements were carried out at low temperature to reduce the contribution of the nonradiative processes to the measured lifetime. Figure 4a shows the spectrally integrated time-resolved traces for Coumarin in micelle structures with and without Ag nanoparticles. The lifetime exhibits a non-exponential decay in both cases, whereas it is fitted well by a biexponential decay function. The average lifetime was determined using the following formula:

$$\langle \tau \rangle = \frac{A_1\tau_1^2 + A_2\tau_2^2}{A_1\tau_1 + A_2\tau_2} \qquad (1)$$

A reduction of $\langle \tau \rangle$ from 2.5 to 1.8 ns in the presence of the metal nanoparticles was observed. We attribute this reduction to the plasmon−exciton coupling. The relatively small but yet significant decrease in the lifetime (~25%)[2,13,15] could be an intrinsic characteristic of our nanohybrid material or be due to the fact that not all dyes can interact efficiently with the MNPs. Indeed, we cannot fully exclude the presence of some residual dyes in the voids among the micelles, which could partially mask the real (and possibly higher) coupling efficiency, thus contributing as fluorescence background.

Nevertheless, the reduction in the emission lifetime can be unambiguously attributed to a quenching mechanism resulting from the short distance (~2−3 nm) plasmon−exciton coupling between dye molecules and metal nanoparticles in the micelle structure. It was indeed demonstrated[2,7−9,13,15] that on this length scale the main interaction process is governed by a nonradiative energy transfer from the dye to the metal nanoparticles. In other words, the close proximity of MNPs provides a new nonradiative channel mediated by the resonant plasmon−exciton interaction, which results in a reduction of the exciton lifetime. The above-mentioned behavior has not been observed in the control experiment with Rhodamine (Figure 4b), ruling out the well-known metallic quenching *via* the electrostatic image charge as predominant interaction, which would affect dyes independent of their emission wavelength.

The observed non-exponential behavior is striking and reveals the presence of additional processes coexisting and competing with radiative recombination. Deeper insight into the underlying physical processes

can be gained from the temporal evolution of the fluorescence spectra. For a quantitative analysis of these processes, we fitted a single Gaussian function to the emission spectrum for every time bin of 100 ps. The energy peak shift, reported in Figure 4c,d, is attributed to a nonradiative Förster-like energy transfer process between the dyes allowing the exciton to diffuse toward lower energy states. This is the result of energy transfer within the inhomogeneously broadened energy distribution in the ensemble of dyes within a micelle. A slower red shift was observed for Coumarin linked to the MNPs (Figure 4c).

This behavior could be attributed to a modification of the transfer efficiency among the molecules due to the presence of the plasmonic resonance as demonstrated in ref 28. Support for the notion on the plasmonic nature of the interaction comes from control experiments carried out using Rhodamine, which rule out the contribution of other processes (chemical alteration, interaction with surface electrons, *etc.*) to the behavior observed.

CONCLUSION

In summary, we synthesized ultrasmall (2−3 nm) and crystalline silver nanocrystals uniformly dispersed together with fluorescent dyes in micelle structures. Our investigation of the nanocomposite substantiates the occurrence of plasmon−exciton interaction affecting the fluorescence temporal behavior of a dye in resonance with the plasmon band (Coumarin), while leaving the emission of a nonresonant dye (Rhodamine) unchanged. Such manipulation possibilities enable tailoring of the opto-electronic properties at the nanoscale, representing the ultimate limit for plasmonic metal particles before the transition to the molecular-like regime, for which a completely different behavior is expected. Furthermore, embedding the constituents into a micelle structure prevents aggregation and protects them in subsequent processing steps (*e.g.*, nanolithography), which are pivotal for many potential applications in nanophotonics, sensing, and biology.

EXPERIMENTAL SECTION

Sample Preparation. A diblock copolymer of polystyrene (PS) and poly(4-vinyl pyridine) (P4VP), PS-*b*-P4VP, with a molecular weight of 12 000 and 9500 g/mol for PS and P4VP, respectively, was purchased from Polymer Source Inc. (Dorval, Canada) and used without further purification. The PS-*b*-P4VP was dissolved in toluene to prepare micelles. Typical concentration was 0.5 wt %, and higher concentrations were used to control the film thickness. The solutions were stirred for 3 h at 70 °C. Coumarin 6H and Rhodamine B were purchased from Exciton (Dayton, OH) and used as received. Organic dyes were added to the micelle solution, which was then stirred for 24 h. Subsequently, silver nitrate ($AgNO_3$) was added to the solution and the solution stirred for an additional 24 h. To prepare thin films on substrates, the micelle solution was mixed with a toluene solution of PS homopolymer (13 200 g/mol, from Polymer Source, Inc.). Thin films were prepared by spin-coating the solution onto precleaned quartz wafers. The dye amount in the thin film samples was controlled to be 0.25 and 0.45 mol %. The thickness of the samples was measured using a NanoSpec/AFT 4150 (Nanometrics Inc.). All of the samples were controlled to be approximately 200 nm in thickness.

Structural Characterization. Transmission electron microscopy (TEM) analysis was carried out on a JEOL 2010F 200 kV Schottky field emission TEM. High-resolution TEM imaging revealed the crystalline nature of the Ag nanoparticles, while *Z*-contrast imaging technique[32] in scanning TEM (STEM) mode in combination with energy-dispersive X-ray spectroscopy (EDS) and EELS enabled confirmation of the elemental composition of the nanoparticles. Special precautions were taken to ensure that no significant beam damage occurred during data acquisition.

Optical Characterization. Steady-state photoluminescence and photoluminescence excitation spectra were measured by using a Hitachi F4500 fluorescence spectrometer with a xenon lamp as excitation source. Time-resolved measurements were performed by using a TOPAS nonlinear frequency mixing modulus pumped by an amplified (3 mJ, 1 kHz) Ti:sapphire mode-locked laser delivering pulses of about 150 fs duration. The photoluminescence was dispersed by a grating with 150 grooves/mm in a 300 mm spectrograph and finally detected using a Hamamatsu C5680 streak camera with 2 ps time resolution. For low-temperature measurements, the samples were mounted in a liquid helium flow cryostat with a helium exchange gas atmosphere.

Acknowledgment. We thank B. Mazenauer and D. Caimi for their technical support, and B. Offrein for stimulating discussions. The research leading to these results has received funding from the IBM's MRC−Visiting Scientist Program and from the European Community's Seventh Framework Programme under Grant Agreement No. 214954 (HERODOT).

REFERENCES AND NOTES

1. Barnes, W. L.; Dereux, A.; Ebbesen, T. W. Surface Plasmon Subwavelength Optics. *Nature* **2003**, *424*, 824–830.
2. Seelig, J.; Leslie, K.; Renn, A.; Kühn, S.; Jacobsen, V.; van de Corput, V. M.; Wyman, C.; Sandoghdar, V. Nanoparticle-Induced Fluorescence Lifetime Modification as Nanoscopic Ruler: Demonstration at the Single Molecule Level. *Nano Lett.* **2007**, *7*, 685–689.
3. Tovmachenko, O. G.; Graf, C.; van den Heuvel, D. J.; van Blaaderen, A.; Gerritsen, H. C. Fluorescence Enhancement by Metal-Core/Silica-Shell Nanoparticles. *Adv. Mater.* **2006**, *18*, 91–95.
4. Ruppin, R. Decay of an Excited Molecule near a Small Metal Sphere. *J. Chem. Phys.* **1982**, *76*, 1681–1684.
5. Kühn, S.; Håkanson, U.; Rogobete, L.; Sandoghdar, V. Enhancement of Single-Molecule Fluorescence Using a Gold Nanoparticle as an Optical Nanoantenna. *Phys. Rev. Lett.* **2006**, *97*, 017402.
6. Bardhan, R.; Grady, N. G.; Cole, J. R.; Joshi, A.; Halas, N. J. Fluorescence Enhancement by Au Nanostructures: Nanoshells and Nanorods. *ACS Nano* **2009**, *3*, 744–752.
7. Anger, P.; Bharadwaj, P.; Novotny, L. Enhancement and Quenching of Single-Molecule Fluorescence. *Phys. Rev. Lett.* **2006**, *96*, 113002.
8. Thomas, M.; Greffet, J.-J.; Carminati, R.; Arias-Gonzalez, J. R. Single-Molecule Spontaneous Emission Close to Absorbing Nanostructures. *Appl. Phys. Lett.* **2004**, *85*, 3863–3865.
9. Sun, G.; Khurgin, J. B.; Soref, R. A. Practical Enhancement of Photoluminescence by Metal Nanoparticles. *Appl. Phys. Lett.* **2009**, *94*, 101103.

10. Pompa, P. P.; Martiradonna, L.; Della Torre, A.; Della Sala, F.; Manna, L.; De Vittorio, M.; Calabi, F.; Cingolani, R.; Rinaldi, R. Metal-Enhanced Fluorescence of Colloidal Nanocrystals with Nanoscale Control. *Nat. Nanotechnol.* **2006**, *1*, 126–130.
11. Lee, J.; Hernandez, P.; Lee, J.; Govorov, A. O.; Kotov, N. A. Exciton–Plasmon Interactions in Molecular Spring Assemblies of Nanowires and Wavelength-Based Protein Detection. *Nat. Mater.* **2007**, *6*, 291–295.
12. Yun, C. S.; Javier, A.; Jennings, T.; Fisher, M.; Hira, S.; Peterson, S.; Hopkins, B.; Reich, N. O.; Strouse, G. F. Nanometal Surface Energy Transfer in Optical Rulers, Breaking the FRET Barrier. *J. Am. Chem. Soc.* **2005**, *127*, 3115–3119.
13. Jennings, T. L.; Singh, M. P.; Strouse, G. F. Fluorescent Lifetime Quenching near $d = 1.5$ nm Gold Nanoparticles: Probing NSET Validity. *J. Am. Chem. Soc.* **2006**, *128*, 5462–5467.
14. Tang, Y.; Ouyang, M. Tailoring Properties and Functionalities of Metal Nanoparticles through Crystallinity Engineering. *Nat. Mater.* **2007**, *6*, 754–759.
15. Dulkeith, E.; Ringler, M.; Klar, T. A.; Feldmann, J.; Javier, A. M.; Parak, W. J. Gold Nanoparticles Quench Fluorescence by Phase Induced Radiative Rate Suppression. *Nano Lett.* **2005**, *5*, 585–589.
16. Brege, J. J.; Hamilton, C. E.; Crouse, C. A.; Barron, A. R. Ultrasmall Copper Nanoparticles from a Hydrophobically Immobilized Surfactant Template. *Nano Lett.* **2009**, *9*, 2239–2242.
17. Novo, C.; Funston, A. M.; Mulvaney, P. Direct Observation of Chemical Reactions on Single Gold Nanocrystals Using Surface Plasmon Spectroscopy. *Nat. Nanotechnol.* **2008**, *3*, 598–602.
18. Turner, M.; Golovko, V. B.; Vaughan, O. P. H.; Abdulkin, P.; Berenguer-Murcia, A.; Tikhov, M. S.; Johnson, B. F. G.; Lambert, R. M. Selective Oxidation with Dioxygen by Gold Nanoparticle Catalysts Derived from 55-Atom Clusters. *Nature* **2008**, *454*, 981–984.
19. Kawata, S.; Inouye, Y.; Verma, P. Plasmonics for Near-Field Nano-Imaging and Superlensing. *Nat. Photonics* **2009**, *3*, 388–394.
20. Ozbay, E. Plasmonics: Merging Photonics and Electronics at Nanoscale Dimensions. *Science* **2006**, *311*, 189–193.
21. Anker, J. N.; Hall, W. P.; Lyandres, O.; Shah, N. C.; Zhao, J.; Van Duyne, R. P. Biosensing with Plasmonic Nanosensors. *Nat. Mater.* **2008**, *7*, 442–453.
22. Haes, A. J.; Chang, L.; Klein, W. L.; Van Duyne, R. P. Detection of a Biomarker for Alzheimer's Disease from Synthetic and Clinical Samples Using a Nanoscale Optical Biosensor. *J. Am. Chem. Soc.* **2005**, *127*, 2264–2271.
23. Sundaramurthy, S. A.; Schuck, P. J.; Conley, N. R.; Fromm, D. P.; Kino, G. S.; Moerner, W. E. Toward Nanometer-Scale Optical Photolithography: Utilizing the Near-Field of Bowtie Optical Nanoantennas. *Nano Lett.* **2006**, *6*, 355–360.
24. Yoon, B.; Huh, J.; Ito, H.; Frommer, J.; Sohn, B.-H.; Kim, J. H.; Thomas, E. L.; Park, C.; Kim, H.-C. Smart Self-Adjustment of Surface Micelles of an Amphiphilic Block Copolymer to Nanoscopic Pattern Boundaries. *Adv. Mater.* **2007**, *19*, 3342–3348.
25. Govorov, A. O.; Bryant, G. W.; Zhang, W.; Skeini, T.; Lee, J.; Kotov, N. A.; Slocik, J. M.; Naik, R. R. Exciton–Plasmon Interaction and Hybrid Excitons in Semiconductor–Metal Nanoparticle Assemblies. *Nano Lett.* **2006**, *6*, 984–994.
26. Hua, X. M.; Gersten, J. I.; Nitzan, A. Theory of Energy Transfer between Molecules near Solid State Particles. *J. Chem. Phys.* **1985**, *83*, 3650–3659.
27. Gersten, J. I.; Nitzan, A. Accelerated Energy Transfer between Molecules near a Solid Particle. *Chem. Phys. Lett.* **1984**, *104*, 31–37.
28. Reil, F.; Hohenester, U.; Krenn, J. R.; Leitner, A. Förster-Type Resonant Energy Transfer Influenced by Metal Nanoparticles. *Nano Lett.* **2008**, *8*, 4128–4133.
29. Zhang, J.; Fu, Y.; Lakowicz, J. R. Enhanced Förster Resonance Energy Transfer (FRET) on a Single Metal Particle. *J. Phys. Chem. C* **2007**, *111*, 50–56.
30. Varnavski, O.; Ramakrishna, G.; Kim, J.; Lee, D.; Goodson, T. Critical Size for the Observation of Quantum Confinement in Optically Excited Gold Clusters. *J. Am. Chem. Soc.* **2010**, *132*, 16–17.
31. Sohn, B.-H.; Yoo, S.-I.; Seo, B.-W.; Yun, S. H.; Park, S.-M. Nanopatterns by Free-Standing Monolayer Films of Diblock Copolymer Micelles with *In Situ* Core–Corona Inversion. *J. Am. Chem. Soc.* **2001**, *123*, 12734–12735.
32. Wang, W.; Asher, S. A. Photochemical Incorporation of Silver Quantum Dots in Monodisperse Silica Colloids for Photonic Crystal Applications. *J. Am. Chem. Soc.* **2001**, *123*, 12528.
33. Nellist, P. D.; Pennycook, S. J. Incoherent Imaging Using Dynamically Scattered Coherent Electrons. *Ultramicroscopy* **1999**, *78*, 111–124.
34. Leroux, F.; Gysemans, M.; Bals, S.; Batenburg, K. J.; Snauwaert, J.; Verbiest, T.; Van Haesendonck, C.; Van Tendeloo, G. Three-Dimensional Characterization of Helical Silver Nanochains Mediated by Protein Assemblies. *Adv. Mater.* **2010**, *22*, 2193–2197.